



31 Landslide susceptibility assessment over large areas is considered a preliminary step for the  
32 planning or design of the most appropriate risk mitigation measures. The use of [statistics and physics](#)  
33 based models is considered a useful tool for landslide susceptibility assessment (Amashi et al., 2019;  
34 Baena et al., 2019; Ciurleo et al., 2019; Hu et al., 2019; Rao et al., 2017; Singh et al., 2019; Xie et al.,  
35 2015). However, the research of these methods was mainly focused on the gully scale. At the same time,  
36 these methods did not focus on the specific principle of material storage, but carried out statistical or  
37 comprehensive analysis on the main factors affecting the landslides distribution.

38 Geomorphic evolution has been one of the important research topics in geomorphology,  
39 hypsometric analysis has been used to deal with erosional topography and the process of landform  
40 development (Bartolini et al., 2003; Li et al., 2011; Lv et al., 2005). Strahler (1952) asserted that  
41 different types of landform have different characteristic shape of their hypsometric curves, dividing  
42 landform into 'young' and 'mature' with the hypsometric integral decreasing. The integral can be used  
43 to indicate the geomorphological evolution state, in this meaning, it can be defined as the evolution  
44 index (EI) of a tributary (Kashani et al., 2019; Qureshi et al., 2019; Strahler, 1952, 1957). Meanwhile,  
45 the hypsometric curves are related to tributary form and erosional process, and are used to interpret  
46 landform development stages (Schumm, 1956; Strahler, 1952, 1957), which can represent the state of  
47 material storage of a tributary. In addition, the relationship between EI and tributary characteristics  
48 changes with scales. For example, the dissection index of tributaries presents various relationships to  
49 EI depending on scale of the tributaries. For the 5th-order tributaries, their correlation is  $r = 0.41$ ,  
50 whereas for the 4th-order, it is  $r = 0.24$ , and it becomes negative correlation for the 3rd-order (Hamza et  
51 al., 2018). Combined with the results of field investigation, this study adopts the tributary scale that  
52 debris flow easily occurs to meet our research need.

53 For a given watershed, especially a small gully in mountains (below 100 km<sup>2</sup> and most below 10  
54 km<sup>2</sup>), the tributaries with different EI present various topographic characteristics. Similarly, significant  
55 difference exists in the distribution of landslides among various tributaries, landslides are frequent in  
56 some tributaries while occasional in others (Baum et al., 2005; Pradhan and Sameen, 2017; Wang et al.,  
57 2006; Wiczorek, 1996). Therefore, the relationship between EI and landslides distribution has special  
58 significance to reveal the landslides distribution in tributaries, which, however, has been gotten little  
59 attention in literatures.

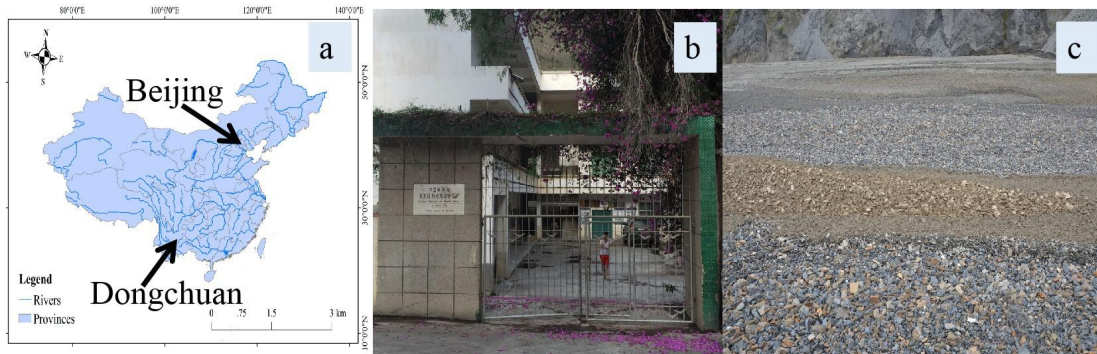
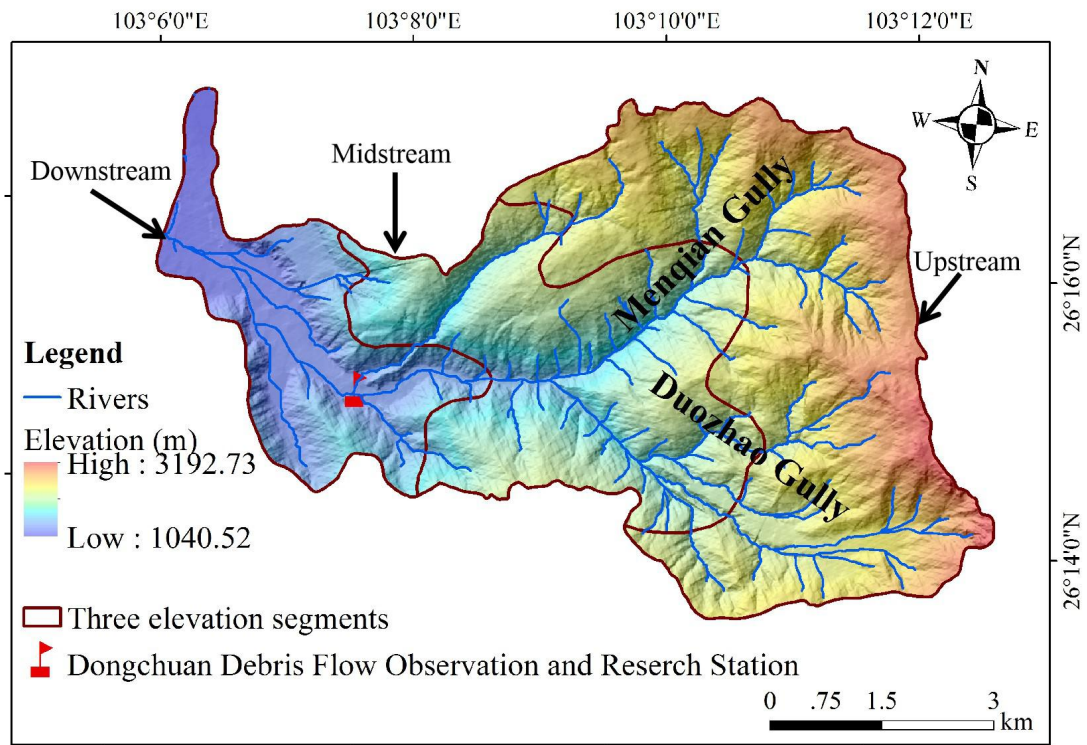
60 In this paper, a case study is conducted in Jiangjia Gully (JJG), where weak and similar lithology,

61 disparate topography, sparse vegetation, and unconsolidated deposits are widely distributed in  
62 tributaries. In addition, the debris flow behavior in JJG are representative, it is known for the high  
63 variety of debris flows; each debris-flow event consists of tens or hundreds surges of different flow  
64 regimes, velocities, discharges, and total volumes (Li et al., 2015; Li et al., 2013; Arai, 2017). In  
65 particular, the surges are composed of different materials, suggesting that they come from different  
66 sources (Xiang et al., 2015). In other words, each debris flow in JJG comes from different tributaries  
67 (Bollschweiler et al., 2007; Li et al., 2012; Li et al., 2013; Li et al., 2015). Generally, the flow surges  
68 are originated from different tributaries and the material supplies are mainly from landslides (including  
69 avalanches, soil failures and other slope processes) (Beguería, 2006). So the study of landslides  
70 distribution in different evolution stages is of great significance to reveal the landslides distribution  
71 characteristics of the tributaries, which can roughly determine the material supply and explain the  
72 formation mechanism of debris flow surges.

## 73 **2 Study area and data collection**

### 74 2.1 The setting of the study area

75 JJG is located in the Xiaojiang River of the Upper Changjiang River. The mainstream channel  
76 length is  $1.39 \times 10^4$  m and the gully area is  $4.84 \times 10^7$  m<sup>2</sup> (Fig. 1). This region undergoes active  
77 neotectonic movement, faults, and folds; and rocks are dominated by slate, dolomite, limestone, basalt  
78 and breccia rocks, which are easily weathered (Gabet and Mudd, 2006). The exposed strata in this gully  
79 is mainly shallow metamorphic rocks of the lower proterozoic Kunyang group, accounting for about  
80 80% of the whole gully area (Wu et al., 1990). Generally, weak lithology, wide faults and sparse  
81 vegetation are the obvious characteristics of the gully, and the tributaries are in steep topography and  
82 intense landslide activity, with wide distribution of quaternary unconsolidated deposits. Loose materials  
83 are widely distributed in the gully and debris flows occur frequently, which are the major material  
84 sources for the debris flows. According to the statistics data, the landslides area reaches 16.4 km<sup>2</sup> that  
85 accounts for 39.7% of the gully area. As well, average annual sediment yield by debris flow is about  
86  $1.54 \times 10^6$  m<sup>3</sup> (Wu et al., 1990; Zhuang et al., 2015).



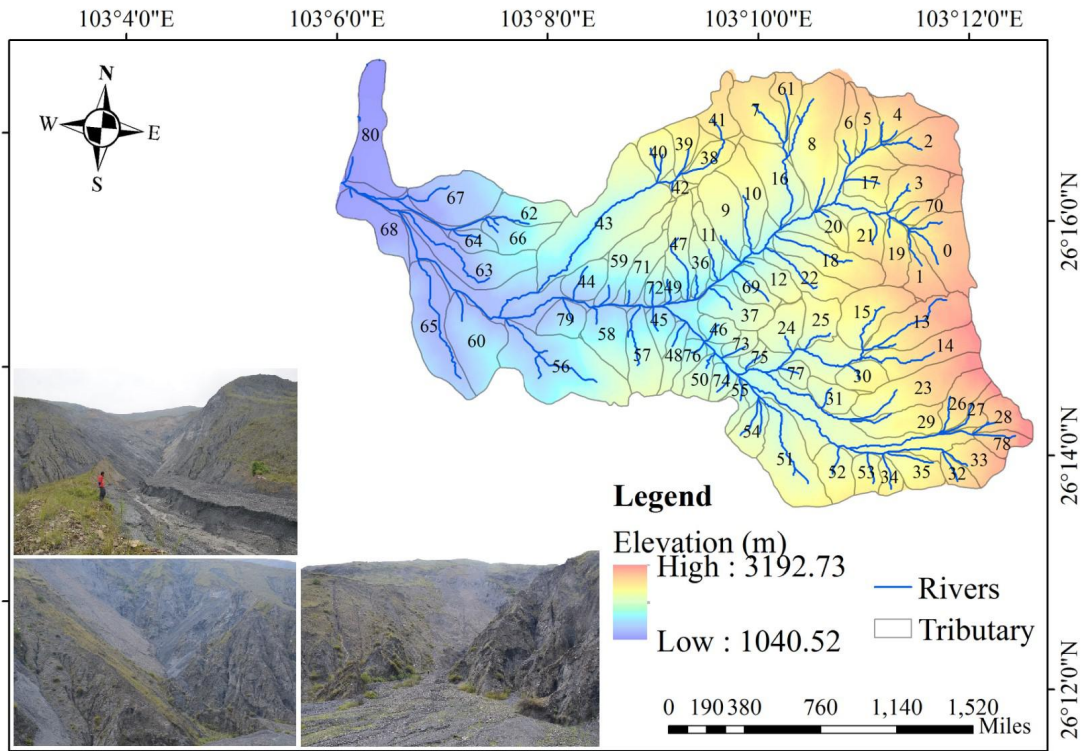
87  
88 **Fig. 1** The location of JJG. a The location of Dongchuan in China. b Dongchuan Debris Flow  
89 Observation and research stations. c Deposition of surges.

90 2.2 Data collection

91 2.2.1 The tributaries divided in JJG

92 Digital elevation model with spatial resolution 10 m is used in this study to generate elevation and  
93 area information, which was purchased in the Sichuan surveying and mapping bureau. 81 tributaries  
94 are abstracted from the watershed of JJG. The tributaries are divided based on field investigation result  
95 that each tributary is a complete unit for observable landslides and debris flows, also according to the  
96 fact that debris flows are prone to occur instead of direct extraction based on the same water collection  
97 threshold. In other words, these tributaries are all conspicuous in surface mass movement and loose  
98 materials are distinguishable on its slope. The tributaries are extracted from the DEM using GIS tool  
99 and also with artificial correction to ensure the accuracy of boundaries (now it is Fig. 3). In principle,

100 the gully can be divided further into smaller tributaries, but that makes little difference for the present  
 101 purpose as to distinguish tributaries. Some tributaries in field are displayed in Fig. 2, obviously, there  
 102 are significant differences among these tributaries The tributary area varies between  $8.7 \times 10^4 \sim 2.07 \times$   
 103  $10^6 \text{ m}^2$  and cover a total area of  $4.62 \times 10^7 \text{ m}^2$ , about 95% of the whole gully. The serial number of  
 104 tributary in subregions is presented in Table 1.



105  
 106 **Fig. 2** The tributaries divided of JJG. Some tributaries in the field are shown on the map.

107 **Table 1** The tributaries distribution in subregions.

Subregion	The No. of tributaries
Menqian Gully	2, 4, 5, 6, 7, 8, 9, 10, 11, 12, 16, 17, 18, 20, 22, 36, 37, 47, 49, 61, 69
Duozhao Gully	13, 14, 15, 23, 24, 25, 26, 27, 28, 31, 32, 33, 34, 35, 45, 46, 48, 50, 51, 52, 53, 54, 55, 73, 74, 75, 76, 77, 78
Upstream	0, 1, 2, 3, 4, 5, 6, 7, 8, 10, 13, 14, 15, 16, 17, 19, 20, 21, 23, 26, 28, 29, 30, 32, 33, 34, 35, 38, 39, 40, 41, 42, 61, 70
Midstream	9, 11, 12, 22, 31, 36, 37, 43, 45, 46, 47, 48, 49, 50, 51, 54, 55, 59, 69, 71, 72, 73, 74, 75, 76, 77
Downstream	44, 56, 58, 60, 62, 63, 64, 65, 66, 67, 68, 79, 80

109 Hypsometric curve for each tributary is calculated. The hypsometric curve is generated by plotting  
110 the relative area along the abscissa and the relative height along the ordinate. The relative height can be  
111 obtained as the ratio of the height of a given contour (h) from the base plane of the stream mouth to  
112 total height of the tributary with reference to the maximum elevation (H), and the relative area is  
113 obtained as the ratio of the area above a particular contour (a) to the total area of the tributary  
114 encompassing the outlet (A) (Strahler, 1952).

115 Hypsometric integral is the area between the hypsometric curve ( $y=h/H$  and  $x=a/A$ ) and  
116 coordinate axis (Strahler, 1952, 1957), which can be defined as the evolution index (EI).

### 117 2.2.3 The extraction of landslides information

118 Quickbird image of 0.61 m resolution is purchased to create an inventory of landslides. The  
119 satellite image is adopted in this study with low cloud shadow coverage, and the aerial coverage of the  
120 cloudy area is 0.09 km<sup>2</sup> in the study area, about 0.18% of the gully. The atmospheric correction and  
121 radiometric correction have been carried out by using the calibration function within the tools of Envi  
122 5.1 software, and 4, 3, 2 bands are combined to false color image stretched of contrast using standard  
123 deviation method. Both landslides number and landslides area are necessary to interpret, so the equal  
124 area projection is adopted, which has less impact on the landslides area. The landslides information  
125 becomes easily extracted on the source image after processing, which is beneficial to the work of visual  
126 interpretation, and thus ensures the accuracy of the results.

127 Landslides are mapped from high resolution satellite data acquired using visual image  
128 interpretation on Arc GIS 10.3 software with false color composites or panchromatic images uniformly  
129 on 1:5000 scale. The individual landslides initiation zones are indicated using polygons. In the case of  
130 complex situations where many landslides are interconnected, it is difficult to identify the individual  
131 initiation zones. Use of high resolution images enables demarcation of clustered landslides as  
132 individual polygons. The minimum size of landslides area extracted is determined as 253.26 m<sup>2</sup>.

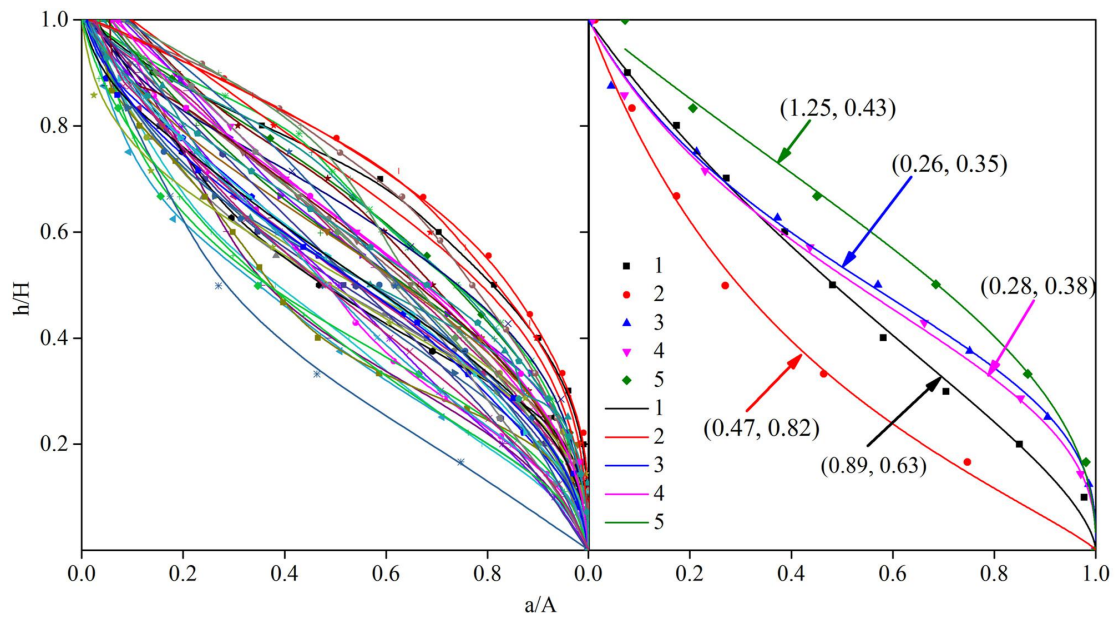
133 In the interpretation process, we make use of the following diagnostic features: the tone, texture,  
134 pattern and shape or form. Meanwhile, direct method, comparison method, integrated reasoning  
135 method and other synthetical methods are always used (Dai and Lee, 2002; Kumar et al., 2017;  
136 Valenzuela et al., 2017). Using the methods above, 906 landslides have been identified, with area  
137 ranging of  $2.53 \times 10^2 \sim 6.7 \times 10^5$  m<sup>2</sup>. In addition, fieldwork was carried out in May and June 2017. We  
138 investigated the location and area of 100 landslides distribution with the GPS instrument, and the

139 accuracy achieves 89.21%. The LA (landslides area) and LN (landslides number) is obtained, they are  
 140 used to analyze the relationship between EI with  $LA_p$  and LD of each tributary, of which  $LA_p$  is  
 141 landslides area in a tributary/ the tributary area (%) and LD is landslides number in a tributary/ the  
 142 tributary area ( $/10^6 m^2$ ).

### 143 3 Evolution division of JJG

#### 144 3.1 Hypsometric analysis

145 The hypsometric curves for tributaries are shown in Fig. 3:



146

147 **Fig. 3** The hypsometric curves of different tributaries.

148 The curves present various types, such as convex, concave and others between them; and these  
 149 can be well fitted by the following function (Strahler, 1957):

$$150 \quad y^{1/n} = k(1-x)/(x+k) \quad (1)$$

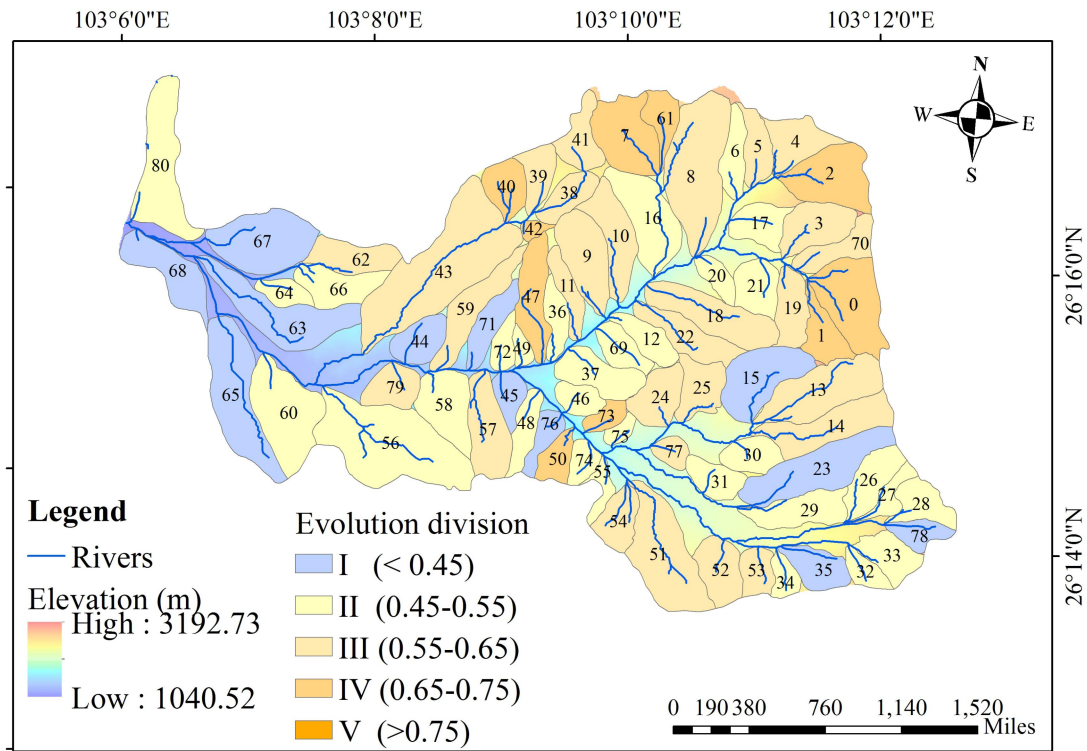
151 Where  $k$  and  $n$  are parameters, with the fitting coefficient  $R^2$  of 0.90 and higher. It is found that higher  
 152 the curve is, greater the  $k$  is. Meanwhile, the curve is rising as  $n$  decreases.

#### 153 3.2 Evolution division of JJG

154 Then the EI of each tributary in JJG is calculated, which varies from 0.32 to 0.84. According to  
 155 Strahler, there are three stages: inequilibrium or youthful stage ( $EI > 0.6$ ), equilibrium or mature stage  
 156 ( $EI$  between 0.3 and 0.6), and monadnock or old stage ( $EI < 0.3$ ) (Strahler 1952). In order to distinguish  
 157 the evolution differences of the tributaries, we conduct a more detailed classification and the EI of  
 158 tributaries in JJG are divided into five groups (Fig. 4):

159 I ( $< 0.45$ ), appears in downstream areas and near the outlet of the gully;

- 160 II (0.45-0.55), occurs mostly in the Duozhao Gully;
- 161 III (0.55-0.65), mostly distributes in midstream and downstream;
- 162 IV (0.65-0.75), mostly in midstream and upstream;
- 163 V (>0.75), mainly distributes in the headwaters of the Menqian Gully;



164 **Fig. 4** The evolution division and EI distribution of tributaries in JYG.

165

166 Moreover, it is found that the EI satisfies the Weibull distribution with the scale parameter of 0.02

167 and the shape parameter of 1.69 (Fig. 5). The small value of scale parameter means that EI is much

168 concentrated and EI of most tributaries in JYG is mainly between 0.5 and 0.6. The shape parameter is

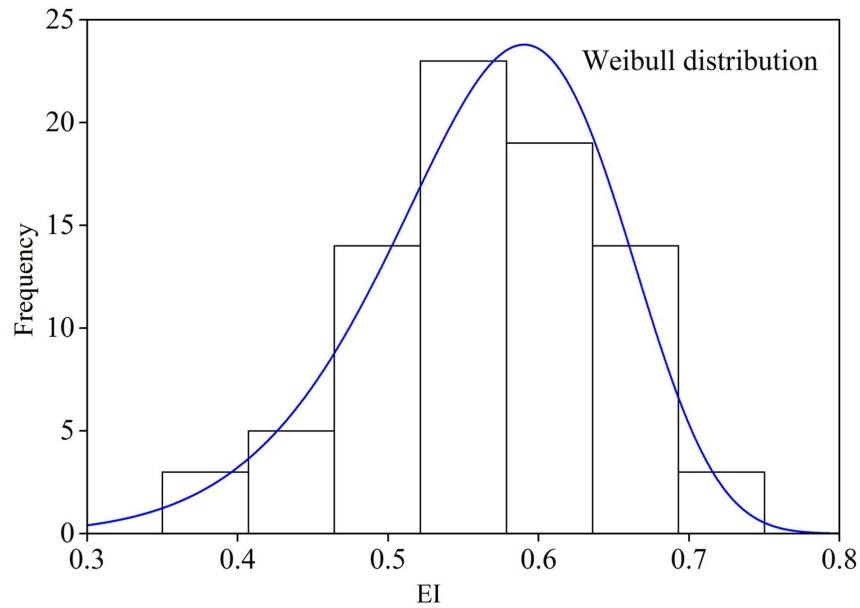
169 more than 1 and the frequency of the tributaries changes rapidly with the increasing of the EI,

170 indicating that there is a great difference among the active tributaries. According to the frequency

171 distribution of EI, the tributaries of JYG is generally in mature and youthful evolution stages, that is the

172 reason why high frequency debris flow occurred in JYG in the past several decades.





173

174

**Fig. 5** The frequency distribution of EI for tributaries in JIG.

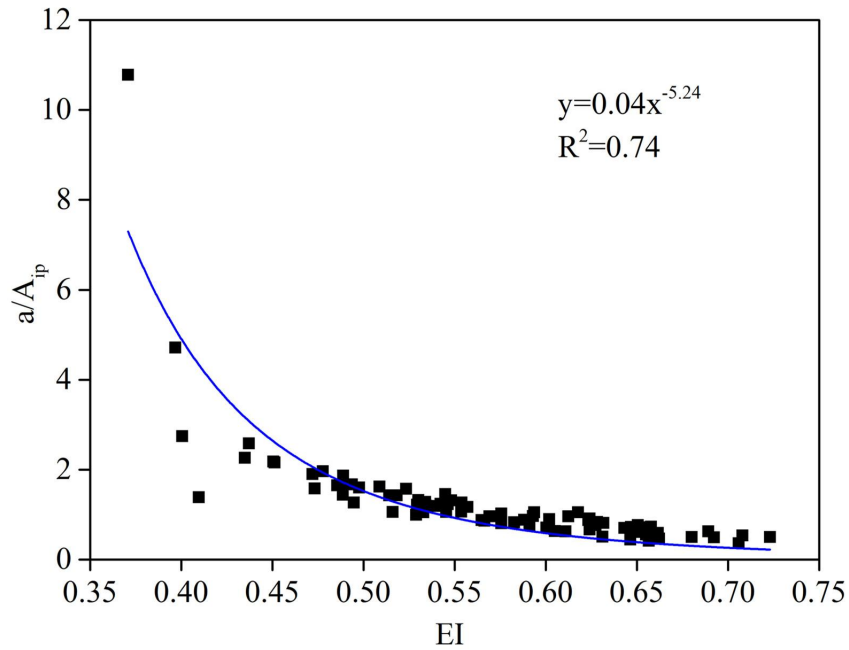
175 3.3 Inflection point of hypsometric curves

176 Obviously, the hypsometric curves exhibit different shapes, which can be featured by the  
 177 inflection point, defined as the zero point of the second derivative of the fitting curve (Eq. 2):

178

$$y'' = \frac{nk^n(k+1)(2x+k-nk-n-1)(1-x)^{n-2}}{(x+k)^{n+2}} \quad (2)$$

179 where  $x$  denotes  $a/A$ , and  $y''=0$  determines the inflection point at  $a/A_{ip}$ . It is found that the  $a/A_{ip}$  varies  
 180 with EI in a power law form (Fig. 6), meaning that the bigger the evolution index is, the lower the  
 181 inflection points of the curves are. The higher the EI value, the lower the inflection point, and this  
 182 implies that there should be more material accumulated in the lower part of the tributary, which are  
 183 relatively easy to join the the debris flow.



184

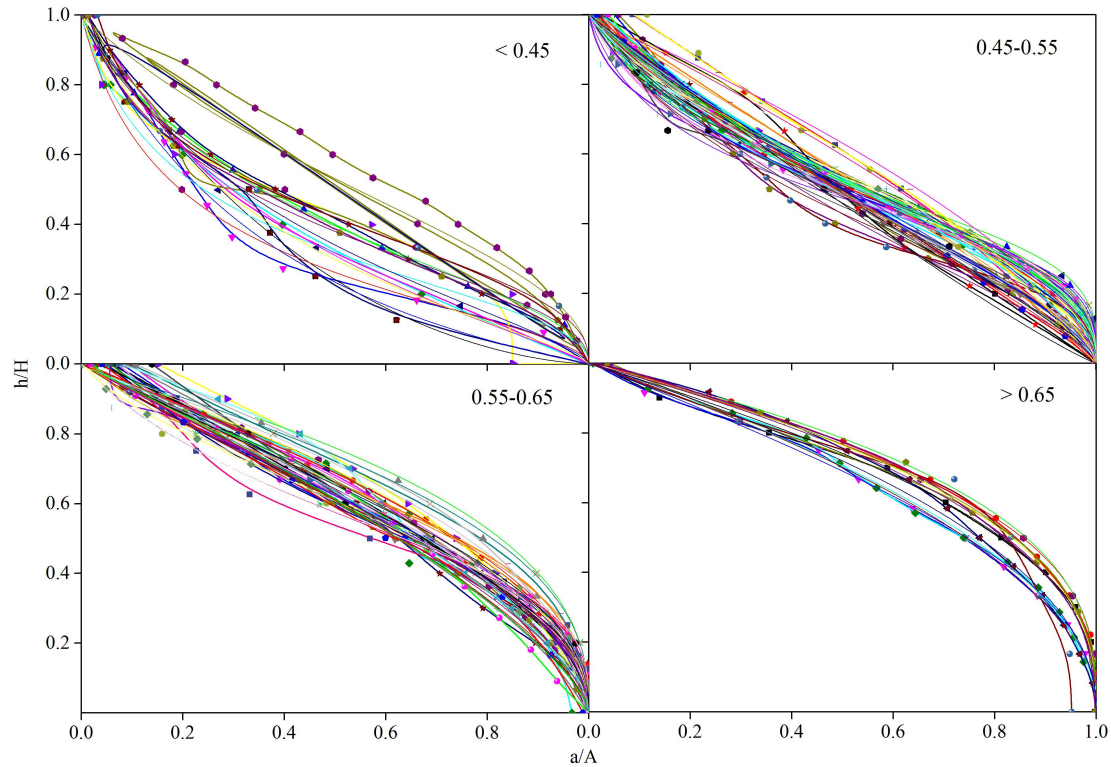
185

**Fig. 6** The relationship between the inflection point and and EI.

186

Moreover, we display the hypsometric curves of different evolution stages in Fig. 7; in particular, the inflection points of the curves (the rectangle in each plot) are displayed in different position of the curves. The inflection point indicates the elevation of a tributary with area varying. It can be seen in Fig. 7 that the larger of the EI is, the smaller of the  $a/A_{ip}$  is. When the point is high, the changing occurs at the high elevation, i.e., mainly in the upstream of the tributary. Since there is no evolution area more than 0.75 in JJG, four major evolution divisions are analyzed.

191

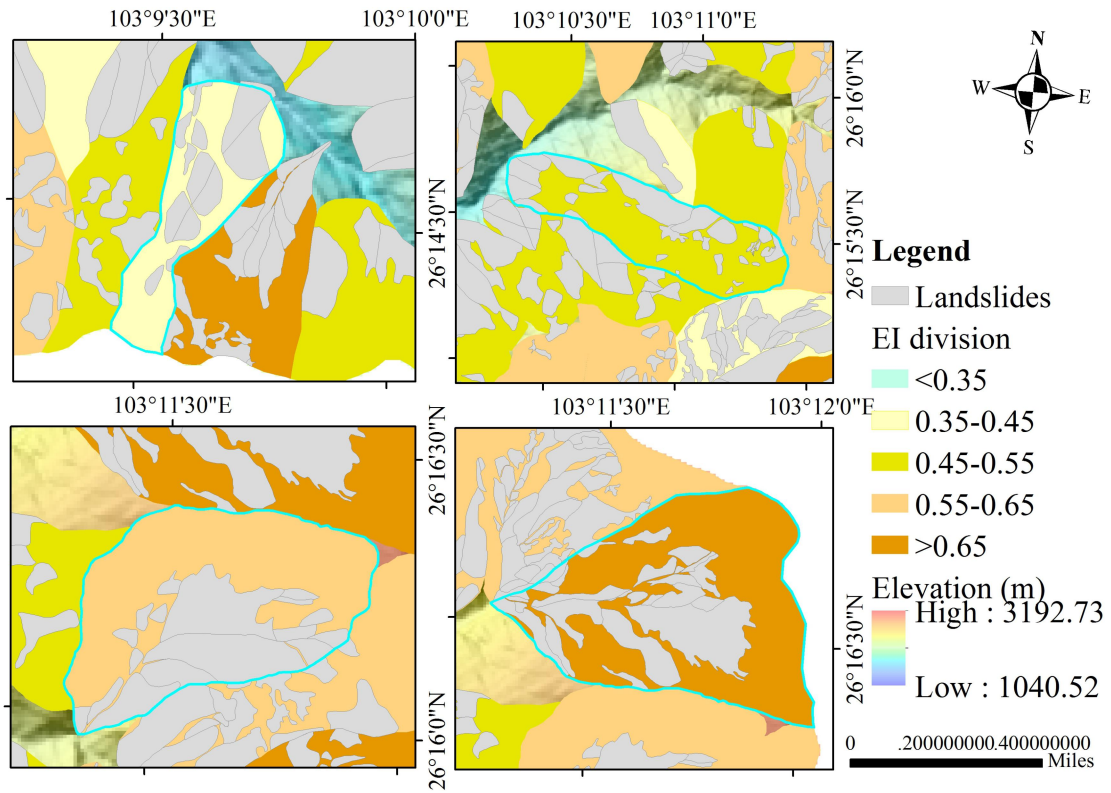


192  
193 **Fig. 7** Hypsometric curves of different EI divisions

194 The evolution curve changes from concave to convex with the increasing of evolution value, and  
195 the convex form of the tributary is more conducive to the material movement of the tributary and more  
196 loose materials are produced.

197 For a given elevation of point, larger area above means that more material are concentrated. For  
198 example, inflection points in EI between 0.45~0.55 are generally higher than those in EI below 0.45,  
199 indicating that more material concentrates in such tributaries, which are more prone to debris flow  
200 activities. Correspondingly, the lower the hypsometric curve is, the more concave the curve is  
201 presented, and the smaller the  $a/A_{ip}$  is, which indicates that the elevation changing in unit area is small,  
202 such a tributary is not conducive to the occurrence of landslides and debris flow activities.

203 Some landslides distribution of tributary in different evolutionary periods is shown in Fig. 8. In  
204 the tributary within the EI range of 0.35-0.45, the landslides distribution is scattered with the large area  
205 and low number, and the tributary is generally concave, which is not conducive to the materials  
206 movement. In addition, with the increasing of the evolutionary value, the landslides number is  
207 increasing and the area is decreasing, and the tributary in high EI division is convex, which is  
208 conducive to the materials movement.



209  
210 **Fig. 8** Some landslides distribution tributaries of different EI divisions

211 **4 Landslides distribution in relation to EI**

212 4.1 Landslides distribution of JJG

213 A total of 906 landslides have been identified, with area ranging from  $2.53 \times 10^2 \text{ m}^2$  to  $6.7 \times 10^5$   
214  $\text{m}^2$ . The spatial distribution of landslides is shown in Fig. 9.

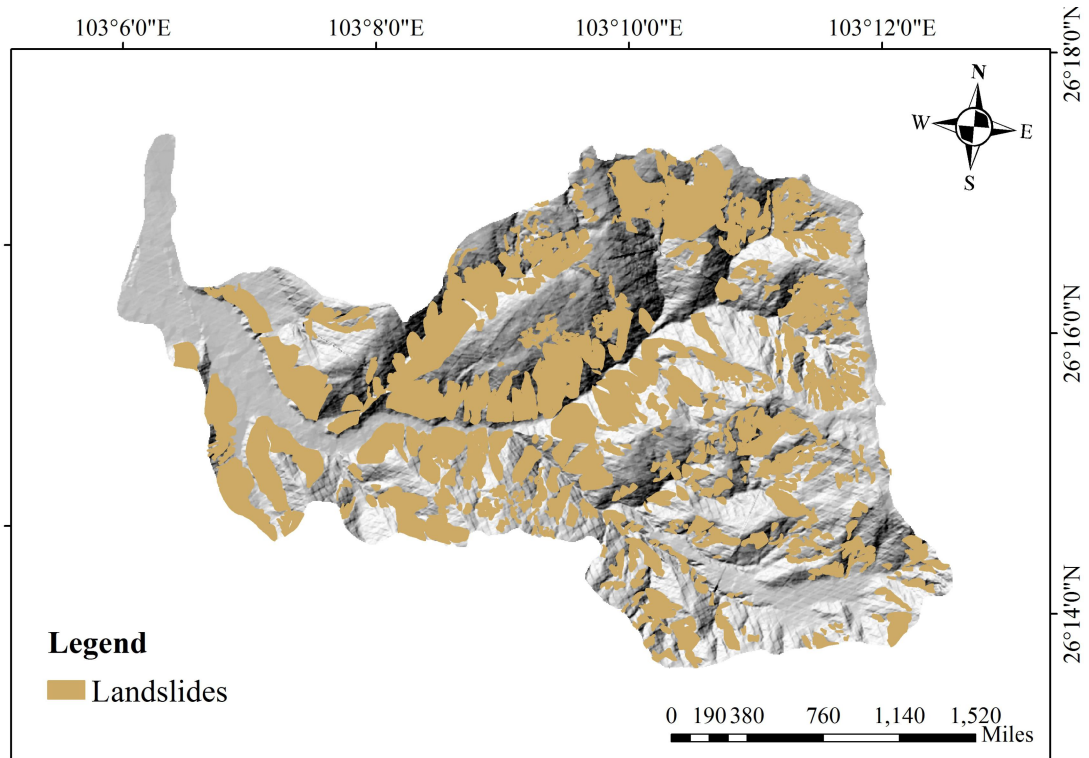


**Fig. 9** Spatial distribution of landslides in JIG.

Landslides are mainly distributed in both sides along the mainstream channels. In details, landslides in Menqian Gully are more concentrated while in Duozhao they are scattering, which is consistent with field observations that landslides are always more frequent in clusters in vulnerable areas.

The landslides distribution in subregions is shown in Table 2. The area of the Menqian gully is smaller than Duozhao gully, the total area and number in Menqian gully is 4.78 km<sup>2</sup> and 274, respectively which is more than Duozhao gully with area 4.18 and number 232. In addition, LA<sub>p</sub> and LD in Menqian gully is more than in Duozhao gully. Since the area of the upstream is the largest and smallest in downstream, it is meaningless to compare the absolute value of the landslides. Now LA<sub>p</sub> and LD in these segments is compared, and LA<sub>p</sub> and LD are both greatest in upstream and smallest in downstream.

**Table 2** The landslides distribution in subregions.

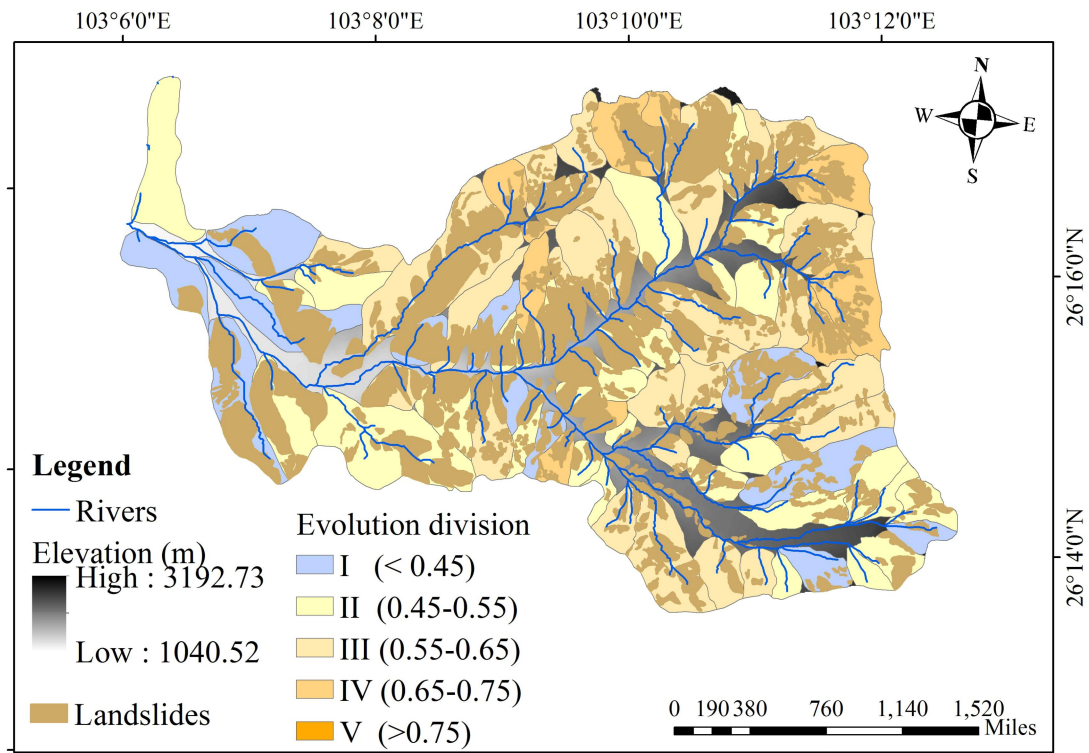
Subregion	The area (km <sup>2</sup> )	The area percentage (%)	Landslides			
			LA (km <sup>2</sup> )	LA <sub>p</sub> (%)	LN	LD (km <sup>2</sup> )
Menqian Gully	10.51	21.72	4.78	45.51	274	26

Duozhao Gully	11.16	23.05	4.18	37.51	232	21
Upstream	16.84	34.80	7.23	42.90	440	26.15
Midstream	10.48	21.65	4.13	39.40	261	25
Downstream	9.71	20.07	3.59	36.91	106	10.90

229 4.2 Landslides distribution in different evolution division

230 4.2.1 The landslides distribution related to evolution stages of all tributaries

231 The evolution division and landslides distribution layers are overlaid to form the spatial  
 232 distribution map, as shown in Fig. 10. It is clear that major of landslides are distributed in subregions of  
 233 III and IV, with EI between 0.55 ~ 0.75.

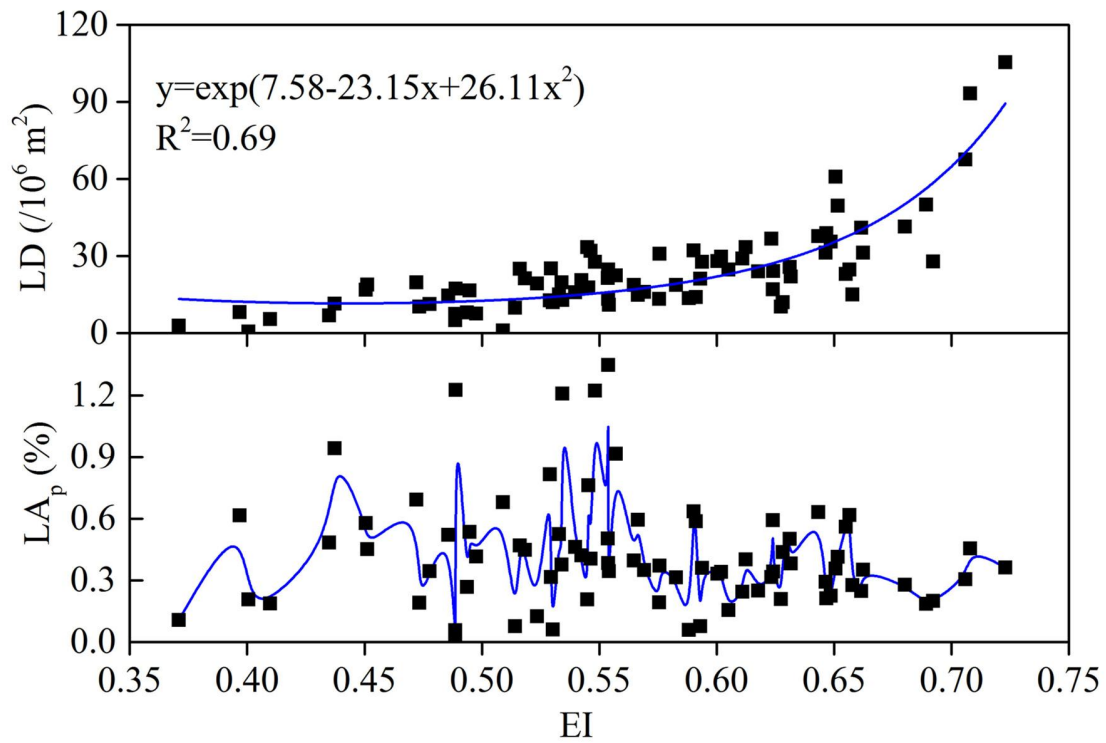


234

235

**Fig. 10** Landslides distribution in various evolution stages.

236 Fig. 11 shows how LD and  $LA_p$  vary with EI. It shows that LD increases exponentially with EI  
 237 increasing, which means that more landslides occur in the tributaries at younger stage. Meanwhile, the  
 238 greater fluctuation of  $LA_p$  is in tributaries with the range of EI less than 0.55, while a smaller  
 239 fluctuation is in tributaries of EI more than 0.55, and the  $LA_p$  is generally smaller than other evolution  
 240 stages in active evolution stage.



241  
242 **Fig. 11** Relationship between landslides and EI.

243 4.2.2 Landslides distribution in typical subregions

244 The major branches of JJG, the gully of Menqian and Duo Zhao, are distinctive in debris flow and  
245 landslides activities. As mentioned above, landslides are more scattering in Duo Zhao and more  
246 concentrated in Menqian. Now we consider how landslides distribute in tributaries in these subregions.

247 Fig. 12 shows that in both gullies LD increases exponentially with EI, almost in the same  
248 exponential function. As for  $LA_p$ , several peaks occur in different EI values in Menqian Gully but only  
249 a single peak occurs (around EI with 0.55) in Duo Zhao Gully, meaning that landslides are widely  
250 distributed in tributaries with  $EI > 0.45$  in Menqian Gully.

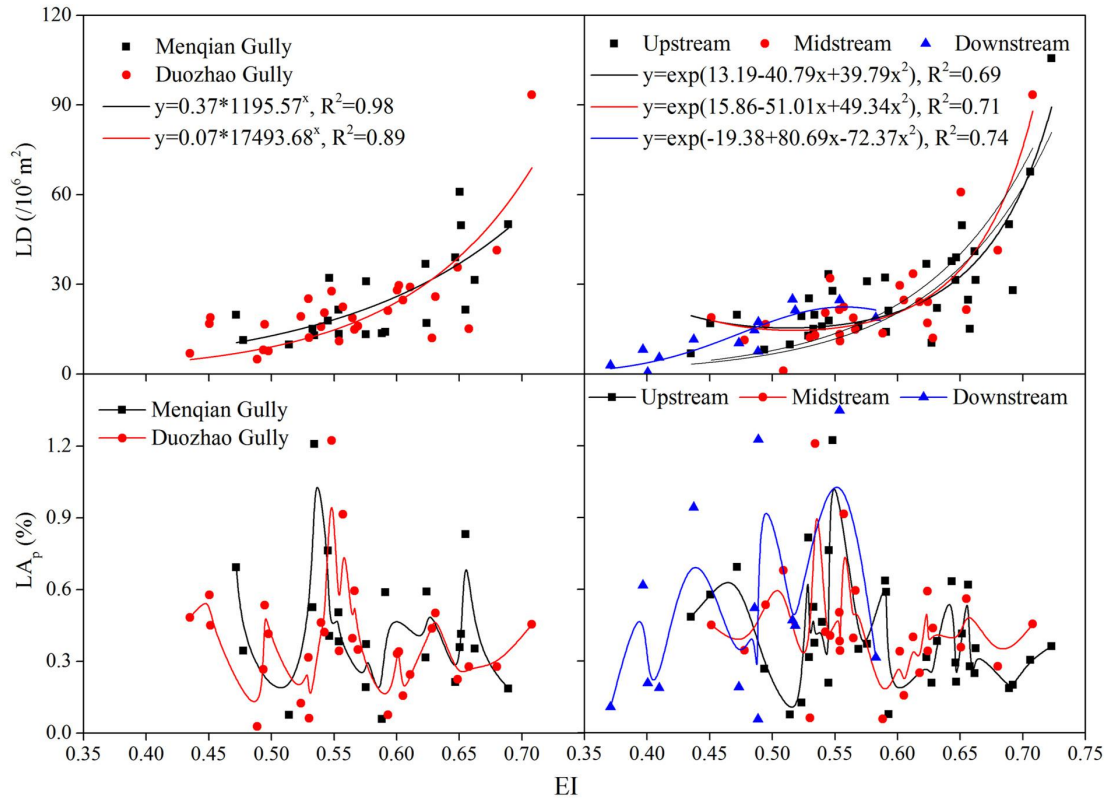


**Fig. 12** Relationship between landslides and EI in subregions.

Similarly, we consider LD and  $LA_p$  in the regions of the upstream, midstream and downstream in JYG that have visible terrain difference, as shown in Fig. 12. Again it is found that LD increases exponentially with EI both in the upstream and midstream.

$LA_p$  mainly increases first and then decreases as EI increases, and the  $LA_p$ -EI curve in the range of less than 0.54 is higher than the range of more than 0.54, which has the similar tendency with the  $LA_p$ -EI curve in all tributaries of JYG. Also the  $LA_p$  in upstream and midstream is higher than downstream, lower  $LA_p$  exists in tributaries at the younger evolutionary stages. Meanwhile, lower LD and larger  $LA_p$  is in the downstream, which is at the old evolution stage, which means that with the occurrence of historical landslides or large landslides in slope surface, the tributary has reached a stable state.

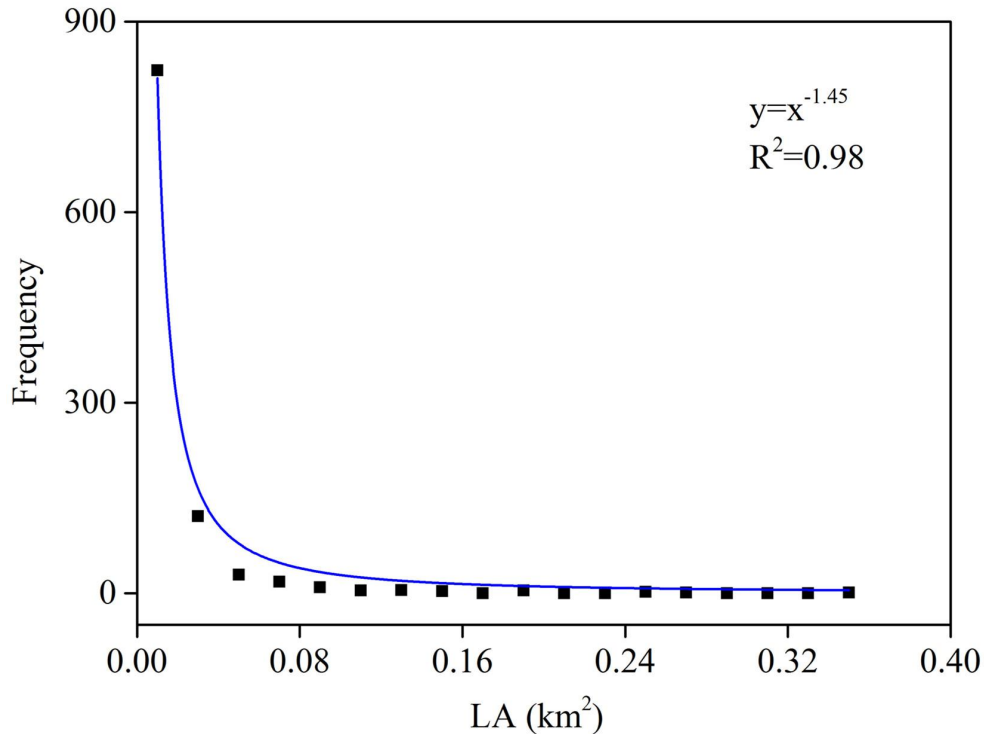
## 5 Discussion

### 5.1 The Power-law distribution of landslides

Power-law frequency-magnitude relationship has been generally observed for landslides at a wide range of size (Hovius et al., 1997; Stark and Hovius, 2001; Malamud et al., 2010), but for a small-scale gully like JYG there is no report in literatures. For the landslides in JYG, the power law is perfectly valid (Fig. 13), with exponent being -1.45, which differs much from the exponent for landslides over large



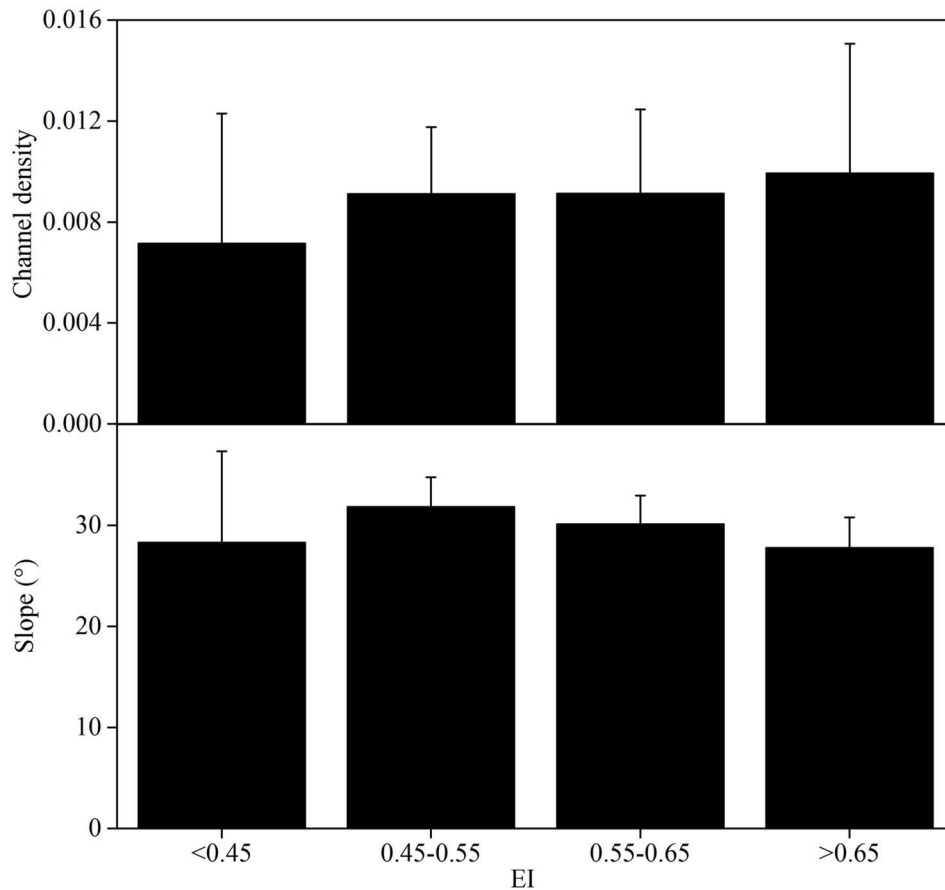
268 scale regions, such as those in the Gorkha area (2.5), the Northridge, California (2.30), and the  
269 Wenchuan area (2.19), and many other regions (Eeckhaut et al., 2007; Lari et al., 2014). The  
270 verification of power law confirms that the landslides area interpreted is reliable.



271  
272 **Fig. 13** The landslide area frequency distribution of JIG.

### 273 5.2 EI and tributary morphological feature

274 As a comprehensive topography index, EI reflects the geomorphology characteristics of the  
275 tributary. Fig. 14 shows how slope varies with EI on average, as it is crucial for landslides and debris  
276 flow formation. The maximal average slope, usually bigger than the friction angle of the soil, occur  
277 mainly between EI of 0.5-0.65, this coincides with range of most landslides distribution, and this also  
278 accounts for the relationship between EI and LD which indicates that EI is related to the number or  
279 frequency of landslides. Meanwhile, the landslides are concentrated in tributaries of class III (EI =  
280 0.55~0.65), and these tributaries are concentrated in the midstream and upstream, mainly in the  
281 Menqian Gully. The landslides distribution in tributaries of different EI quantitatively reveals spatial  
282 heterogeneity distribution. The spatial distinction of landslides distribution results from the diverse  
283 evolution stages of tributaries, which provides a heterogeneous background for material supplying in  
284 gully. The spatial heterogeneity distribution can reveal the reason why landslides are frequent in some  
285 tributaries while occasional in others, thus roughly to predict the landslides activity of tributaries,  
286 which is of great significance to the comprehensive management of small watershed.



287

288 **Fig. 14** The variation of the tributary morphological feature in different evolution stages.

289 Debris flow converging from tributaries into mainstream channel depends on the flow routes, or  
 290 the stream length of each tributary, and this can be described by the channel density (i.e., the length in  
 291 unit area of a region). Fig. 15 shows the density variation with EI, indicating that the channel density of  
 292 tributary is increasing as EI rises, which is conducive to the occurrence of debris flow activity.

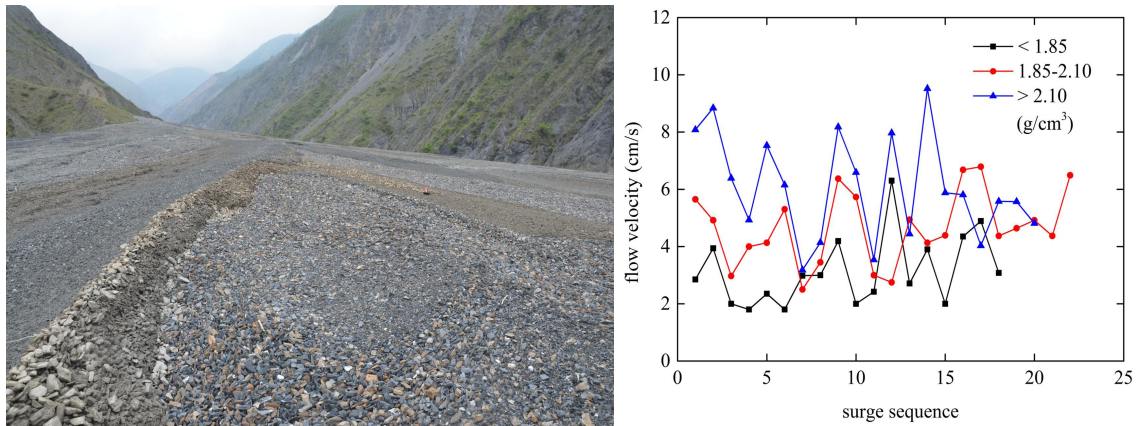
293 Then the tributaries of EI between 0.5 and 0.65 provide favorable condition both for landslides  
 294 and flow convergence, and thus facilitate the forming and developing of debris flows.

295 5.3 Implication in debris flow surges

296 The most remarkable features of debris flow in JJG are the high frequency in occurrence and great  
 297 variety of flow regime and magnitude. Each occurrence contains tens to hundreds of surges (Li et al.,  
 298 2012); the surges are separated in time and space, and different from one another in density, velocity,  
 299 and sediment concentration. The variation of flow velocity with density is shown in Fig. 15, which  
 300 contains surges in one single event on July 12, 2017.

301 The great variety of surges densities, with different material compositions, can be attributed to  
 302 different sources; this means that even a single surge material comes from different tributaries in most

303 cases (Webb et al., 1989). As observed in the last decades, debris flows almost come from the north  
304 branch, the Menqian Gully, while the south branch, the Duo Zhao Gully, is often silent. This presents the  
305 gross distinction of material and landslides activities in JJG, which further implies that there must be  
306 more differences in tributaries.



307

308 **Fig. 15** Debris flow surges deposit in the mainstream of JJG.

309 The spatial heterogeneity of tributary distribution reveals the variety of debris flow sources. As it  
310 is difficult to observe the debris flows of each tributary, we usually see the convergence debris flows  
311 from multiple sources. Debris flow surges always present the characteristic of diverse forms from the  
312 perspective of material supplies (Li et al., 2015), and this can be attributed to the spatial heterogeneity  
313 of evolution and landslides activity of tributaries as discussed above.

314 Previous studies usually consider debris flows activity on the gully scale and ignore the  
315 distinction on tributary scale (Chen and Wang, 2017; Malet et al., 2004), they cannot tell the feature of  
316 debris flows from multiple sources and undergoing diverse tributaries processes, such as initiation on  
317 slope, flow downwards in tributary channel, and confluence into the mainstream, all closely related to  
318 the tributary feature.

319 Besides, the formation of debris flow is activated by rainfall (Chen et al., 2006; Fuchu et al., 1999;  
320 Fusco et al., 2017; Kuo and Chuan, 2007; McArdell et al., 2007; Reneau and Dietrich, 1987; Tan and  
321 Han, 1992), different rainfall intensity and amount is in different tributaries, which adds more diversity  
322 to the surges. The factor of precipitation will be the next study to consider and understand the  
323 formation mechanism of debris flow surges.

#### 324 5.4 General application of EI for landslide source identification

325 The case study in JJG provides a relationship between EI and landslides distribution; the

326 traditional methods make a comprehensive analysis of various influencing factors of landslides  
327 (Amashi et al., 2019; Baena et al., 2019; Ciurleo et al., 2019; Hu et al., 2019; Rao et al., 2017; Singh et  
328 al., 2019; Xie et al., 2015), ignoring the landslides distribution mechanism itself, while this paper  
329 focuses on the analysis of the landslides distribution state itself in tributary, so this method can be  
330 generally applied to identify landslide sources in more general cases. For example, the Wenchuan  
331 earthquake has about 11,000 individual landslide points (Gorum et al., 2011), and it is found that these  
332 landslides are distributed mainly in relatively high EI tributaries (Tian et al., 2019; Xiang et al., 2015).  
333 The EI values for the landslide sources are also subject to the Weibull distribution (Fig. 16), which is  
334 similar to the case of JJG. In comparison, in JJG, EI of tributaries satisfies the Weibull distribution with  
335 the scale and shape parameter for JJG case are respectively of 0.02 and 1.69, while for, this is  
336 comparable to the EI distribution of tributaries in the Wenchuan region where the scale and shape  
337 parameter is 0.53 and 11.73, respectively. The scale parameter can reflect the EI range of variation,  
338 which varies between 0.38 and 0.64 in the Wenchuan area and betweenem 0.37 and 0.73 in JJG. The  
339 difference here can be attributed that a number of tributaries in JJG having no landslides, while in  
340 Wenchuan, only tributaries having landslides distribute in almost every tributary are taken into account,  
341 which means the concentration of EI. This also implies that landslides occur in tributaries within a  
342 relatively narrow range of EI. More important point is the difference between shape parameters, the  
343 bigger shape parameter in Wenchuan region means that the curve is to the right more than in JJG,  
344 implying that the earthquake is inclined to induce more landslides in tributaries of big EI. As JJG is of  
345 tributaries with wide range evolution stages, we choose it as the study area to reveal the mechanism of  
346 landslides distribution.

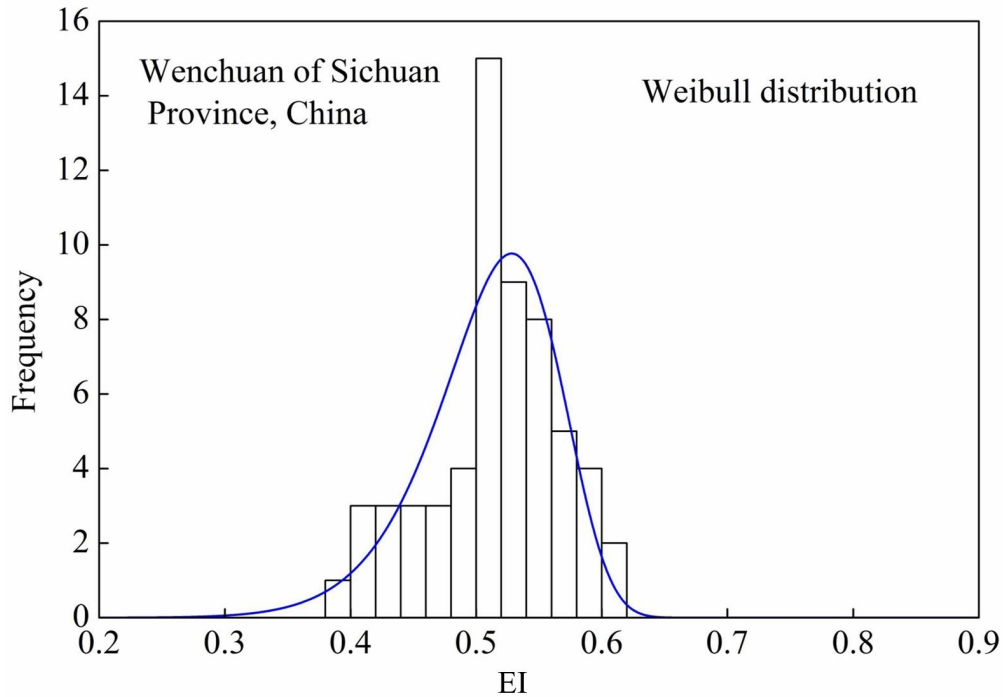


**Fig. 16** The EI frequency distribution of Wenchuan in Sichuan province.

## 6 Conclusions

This study has revealed the spatial heterogeneity of landslides distribution in tributaries of different evolution stages. It is found that most landslides are distributed in the relative young tributaries (with evolution index between 0.5 ~ 0.6). Generally, the LD increases exponentially with EI and the  $LA_p$  is concentrated in EI between 0.5 and 0.6, in accordance with the general landslides distribution. The spatial heterogeneity of landslide distribution provides the background for the high variety and intermittency of debris flows in JJG.

Meanwhile, the EI satisfies the Weibull distribution, such distribution feature also occurs in the tributaries of landslides induced by the Wenchuan earthquake. This implies that the EI can be taken as an indicator for identifying landslide sources in mountainous watersheds.

## Acknowledgments

This research is supported by the Strategic Priority Research Program of the Chinese Academy of Sciences (Grant No.XDA23090202) and the Key International S&T Cooperation Academy of Sciences (grant no. 2016YFE0122400).

## References

366 Amashi, A. R., Hulagabali, A. M., Solanki, C. H., Solanki, G. R., and Dodagoudar.: Landslide Risk  
367 Assessment and Mitigation—A Case Study. Conference paper 2019.

368 Arai, M.: A research on unsteady period of debris flow surges. EGU General Assembly Conference  
369 Abstracts 19, 10715, 2017.

370 Baena, J. A. P., Scifoni, S., Marsella, M., Gianfilippo, D. A., and Clemente, I. F.: Landslide  
371 susceptibility mapping on the islands of Vulcano and Lipari (Aeolian Archipelago, Italy), using a  
372 multi-classification approach on conditioning factors and a modified GIS matrix method for areas  
373 lacking in a landslide inventory. *Landslides* 2019.

374 Bartolini, C., D'Agostino, N., and Dramis, F.: Topography, exhumation, and drainage network  
375 evolution of the apennines. *Episodes* 26, 212-216, 2003.

376 Baum, R. L., Coe, J. A., Godt, J. W., Harp, E. L., Reid, M. E., Savage, W. Z., Schulz, W. H., Brien, D.  
377 L., Chleborad, A. F., and McKenna, J. P.: Regional landslide-hazard assessment for seattle,  
378 washington, USA. *Landslides* 2, 266-279, 2005.

379 Beguería, S.: Changes in land cover and shallow landslide activity: A case study in the spanish  
380 pyrenees. *Geomorphology* 74, 196-206, 2006.

381 Berger, C., Mc Ardell, B. W., and Schlunegger, F.: Sediment transfer patterns at the illgraben catchment,  
382 switzerland: Implications for the time scales of debris flow activities. *Geomorphology* 125,  
383 421-432, 2011.

384 Blahut, J., Westen, C. J. V., and Sterlacchini, S.: Analysis of landslide inventories for accurate  
385 prediction of debris-flow source areas. *Geomorphology* 119, 36-51, 2010.

386 Bollschweiler, M., Stoffel, M., Ehmis, M., and Monbaron, M.: Reconstructing spatio-temporal  
387 patterns of debris-flow activity using dendrogeomorphological methods. *Geomorphology* 87,  
388 337-351, 2007.

389 Chen, C. Y., and Wang, Q.: Debris flow-induced topographic changes: Effects of recurrent debris flow  
390 initiation. *Environmental monitoring and assessment* 189, 449, 2017.

391 Chen, H., Dadson, S., and Chi, Y. G.: Recent rainfall-induced landslides and debris flow in northern  
392 taiwan. *Geomorphology* 77, 112-125, 2006.

393 Ciurleo, M., Mandaglio, M. C., and Moraci, N.: Landslide susceptibility assessment by TRIGRS in a  
394 frequently affected shallow instability area. *Landslides* 16(1):175-188, 2019.

395 Dai, F., and Lee, C.: Landslide characteristics and slope instability modeling using gis, lantau island,

396 hong kong. *Geomorphology* 42, 213-228, 2002.

397 Eeckhaut, M. V. D., Poesen, J., Govers, G., Verstraeten, G., and Demoulin, A.: Characteristics of the  
398 size distribution of recent and historical landslides in a populated hilly region. *Earth & Planetary*  
399 *Science Letters* 256, 588-603, 2007.

400 Fuchu, D., Lee, C., and Sijing, W.: Analysis of rainstorm-induced slide-debris flows on natural terrain  
401 of lantau island, hong kong. *Engineering Geology* 51, 279-290, 1999.

402 Fusco, F., Allocca, V., and Vita, P. D.: Hydro-geomorphological modelling of ash-fall pyroclastic soils  
403 for debris flow initiation and groundwater recharge in campania (southern italy). *Catena* 158,  
404 235-249, 2017.

405 Gabet, E. J., and Mudd, S. M.: The mobilization of debris flows from shallow landslides.  
406 *Geomorphology* 74, 207-218, 2006.

407 Gorum, T., Fan, X. M., Westen, C. J. V., Huang, R. Q., Xu, Q., Tang, C., and Wang, G. H.: Distribution  
408 pattern of earthquake-induced landslides triggered by the 12 May 2008 Wenchuan earthquake.  
409 *Geomorphology* 133(3-4):0-167, 2011.

410 Hamza, V., Prasannakumar, V., and Pratheesh, P.: Landform evaluation through hypsometric  
411 characterisation: an example from selected river basin in southern western ghats, india 73, 4,  
412 2018.

413 Hovius, N., Stark, C. P., and Allen, P. A.: Sediment flux from a mountain belt derived from landslide  
414 mapping. *Geology* 25, 231-234, 1997.

415 Hu, M., Liu, Q., and Liu, P.: Susceptibility Assessment of Landslides in Alpine-Canyon Region Using  
416 Multiple GIS-Based Models. *Wuhan University Journal of Natural Sciences* 24(3):257-270, 2019.

417 Huggel, C., Clague, J. J., and Korup, O.: Is climate change responsible for changing landslide activity  
418 in high mountains? *Earth Surface Processes and Landforms* 37, 77-91, 2012.

419 Wu, J. s., Kang, Z. C., Tian, L. Q., and Zhang, S. C.: Debris flow observation in jiangjia gully, Yunnan  
420 1990.

421 Kashani, R., Partabian, A., and Nourbakhsh, A.: Tectonic implication of geomorphometric analyses  
422 along the Saravan Fault: evidence of a difference in tectonic movements between the Sistan  
423 Suture Zone and Makran Mountain Belt. *Journal of Mountain Science* 16(05):78-89, 2019.

424 Kumar, D., Thakur, M., Dubey, C. S., and Shukla, D. P.: Landslide Susceptibility Mapping &  
425 Prediction using Support Vector Machine for Mandakini River Basin, Garhwal Himalaya, India.

426 Geomorphology 295, 2017.

427 Kuo, L., and Chuan, T.: Progress in research on debris flow hazard assessment. Journal of  
428 Catastrophology 1, 023, 2007.

429 Langebein, W. B., and Basil, W.: Topographic characteristics of drainage basins. USGS Water Supply  
430 Paper 947-C, 1947.

431 Lari, S., Frattini, P., and Crosta, G. B.: A probabilistic approach for landslide hazard analysis.  
432 Engineering Geology 182, 3-14, 2014.

433 Li, Y., Su, P. C., and Su, F. H.: Debris flow as a spatial poisson process. Journal of Mountain Science  
434 29, 586-590, 2011 (In Chinese).

435 Li, Y., Liu, J. J., Hu, K. H., and Su, P. C.: Probability distribution of measured debris-flow velocity in  
436 jiangjia gully, yunnan province, china. Natural hazards 60, 689-701, 2012.

437 Li, Y., Zhou, X. J., Su, P. C., Kong, Y. D., and Liu, J. J.: A scaling distribution for grain composition of  
438 debris flow. Geomorphology 192, 30-42, 2013.

439 Li, Y., Liu, J. J., Su, F. H., Xie, J., and Wang, B. L.: Relationship between grain composition and debris  
440 flow characteristics: A case study of the jiangjia gully in china. Landslides 12, 19-28, 2015.

441 Lv, X. J., Liu, X. L., and Su, P. C.: The Area-altitude Analysis on the Evolution Stage of Debris Flow  
442 Ravines :Taking Daqu River as an Example. Journal of Mountain Science 23, 336-341, 2005 (In  
443 Chinese).

444 Malet, J. P., Maquaire, O., Locat, J., and Remaître, A.: Assessing debris flow hazards associated with  
445 slow moving landslides: methodology and numerical analyses. Landslides 1, 83-90, 2004.

446 Martha, T. R., Roy, P., Mazumdar, R., Govindharaj, K. B., and Kumar, K. V.: Spatial characteristics of  
447 landslides triggered by the 2015 m w, 7.8 (gorkha) and m w, 7.3 (dolakha) earthquakes in  
448 nepal. Landslides 1-8, 2016.

449 McArdell, B. W., Bartelt, P., and Kowalski, J.: Field observations of basal forces and fluid pore  
450 pressure in a debris flow. Geophysical Research Letters 34, 248-265, 2007.

451 Malamud, B. D., Turcotte, D. L., Guzzetti, F., and Reichenbach, P.: Landslide inventories and their  
452 statistical properties, Earth Surface Processes & Landforms 29, 687-711, 2010.

453 Pike, R. J., and Wilson, S. E.: Elevation-relief ratio, hypsometric integral, and geomorphic area-altitude  
454 analysis. Geological Society of America Bulletin 82, 1079-1084, 1971.

455 Pradhan, B., and Sameen, M. I.: Landslide susceptibility modeling: Optimization and factor effect



456 analysis. Laser scanning applications in landslide assessment, Springer 115-132, 2017.

457 Qureshi, J., Mahmood, S. A., Masood, A., Khalid, P., and Kaukab, I. S.: DEM and GIS-based  
458 hypsometric analysis to study tectonics and lithologies in southern Suleiman fold and thrust belt  
459 (Balochistan–Pakistan). *Arabian Journal of Geosciences* 12(5):144, 2019.

460 Rao, J., Shen, J., Tang, X. B., and FU, X. D.: Risk Assessment of Landslide Based on Fuzzy  
461 Comprehensive Evaluation and Information Entropy. *Journal of Yangtze River Scientific Research*  
462 Institute 2017.

463 Reneau, S. L., and Dietrich, W. E.: The importance of hollows in debris flow studies; examples from  
464 marin county, california. *Reviews in engineering geology* 7, 165-180, 1987.

465 Schumm, S. A.: Evolution of drainage systems and slopes in badlands at Perth Amboy, New Jersey[J].  
466 *Bulletin of the Geological Society of America* 67, 597-646, 1956.

467 Singh, A., Kanungo, D. P., and Pal, S.: Physical vulnerability assessment of buildings exposed to  
468 landslides in India. *Natural Hazards* 2019.

469 Strahler, A.: Hypsometric analysis of erosional topography. *Bulletin of Geol. Soc. of America* 63,  
470 1117–1142, 1952.

471 Stark, C. P., and Hovius, N.: The characterization of landslide size distributions. *Geophysical Research*  
472 *Letters* 28, 1091-1094, 2001.

473 Strahler, A. N.: Quantitative analysis of watershed geomorphology. *Eos, Transactions American*  
474 *Geophysical Union* 38, 913-920, 1957.

475 Tan, W. P., and Han, Q. Y.: Study on regional critical rainfall indices of debris flow in Sichuan province.  
476 *Journal of catastrophology* 7, 37-42, 1992.

477 Tian, X. F., Su, F. H., Zhang, J. Q., Liu, J. J., and Li, Yong.: Frequency distribution of landslides in the  
478 Wenchuan earth quake area. *Journal of Mountain Science*.

479 Valenzuela, P., Domínguez-Cuesta, M. J., García, M. A. M., and Jiménez-Sánchez, M.: A  
480 spatio-temporal landslide inventory for the NW of Spain: BAPA database. *Geomorphology* 293,  
481 11-23, 2017.

482 Wang, C., Esaki, T., Xie, M., and Qiu, C.: Landslide and debris-flow hazard analysis and prediction  
483 using gis in minamata–hougawachi area, japan. *Environmental Geology* 51, 91-102, 2006.

484 Webb, R. H., Pringle, P. T., and Rink, G. R.: Debris flows from tributaries of the colorado river, grand  
485 canyon national park, arizona. *United States Geological Survey, Professional Paper* 1492, 1989.

486 Wieczorek, G. F.: Landslide triggering mechanisms. *Landslides: Investigation and mitigation* 247,  
487 76-90, 1996.

488 Wieczorek, G. F., and Glade, T.: Climatic factors influencing occurrence of debris flows. *Debris-flow*  
489 *Hazards and Related Phenomena*. Springer Berlin Heidelberg, pp. 325-362, 2005.

490 Wu, J., Kang, Z., Tian, L., and Zhang, S.: Observation and research of debris flow in Jiangjiagou  
491 Ravine, Yunnan Province. Science Pressing, Beijing, pp. 67–145, 1990.

492 Xiang, L. Z., Li, Y., Chen, H. K., Su, F. H., and Huang, X.: Sensitivity analysis of debris flows based  
493 on basin evolution. *Resources and environment of the Yangtze river basin* 24, 1984-1992, 2015 (In  
494 Chinese).

495 Xie, X., Wei, F., Zhang, J., and Shi, Y.: Application of Projection Pursuit Model to Landslide Risk  
496 Classification Assessment. *Earth Science* 2015.

497 Zhuang J. Q., Cui, P., Wang, G. H., Chen, X. Q., and Guo, X. J.: Rainfall thresholds for the occurrence  
498 of debris flows in the Jiangjia Gully, Yunnan Province, China. *Engineering Geology* 195, 335-346,  
499 2015.